

# Experimental Study on the Desulfurization, Denitration, and Dust Removal Characteristics of Ceramic Fiber Filter Tubes

Yilin Song, Yize Zhang, Qiwei Wu, Di Kang, Shiyi Guo, and Hao Zhou\*



Cite This: *Energy Fuels* 2022, 36, 3715–3726



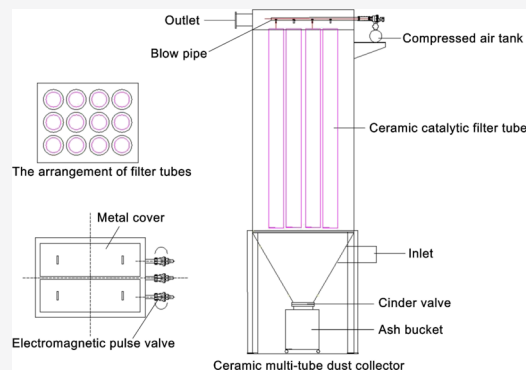
Read Online

ACCESS |

Metrics & More

Article Recommendations

**ABSTRACT:** In this study, we used a vacuum centrifugal suction filtration technology to develop ceramic fiber filter tubes with a high strength and low pressure drop. The V, Mo nanocatalyst slurry with metatitanic acid as the carrier precursor was implanted into a ceramic fiber filter tube. By injecting  $\text{NaHCO}_3$  upstream, the desulfurization, denitrification, and dust removal characteristics of the ceramic catalytic filter tubes from 180 to 330 °C were investigated. The effects of the  $\text{NO}_x$  concentration, the ammonia–nitrogen ratio, the filtration velocity in the ceramic filter tube, and the reaction temperature on the separate denitrification process were investigated. In addition, the effects of the filtration velocity, the reaction temperature, and the sodium–sulfur ratio in the ceramic filter tube on the simultaneous desulfurization and denitrification process were also studied. At 330 °C, the highest denitration efficiency was 97.62%, and the highest desulfurization efficiency was 94.23%.



## 1. INTRODUCTION

The Chinese Government had issued an ultralow emission standard policy for coal-fired power plants, requiring that the total emissions of particulate matter,  $\text{NO}_x$ , and  $\text{SO}_x$  should not exceed 10, 50, and 35  $\text{mg}/\text{m}^3$  by the end of 2020, respectively.<sup>1</sup> Due to the environmental requirements, fly ash particles and pollutants from coal or biomass combustion must be removed. The current solution for flue gas purification is to remove particulate matter,  $\text{NO}_x$ , and  $\text{SO}_x$  from the dust removal unit, denitration unit, and desulfurization unit, respectively. Desulfurization technologies mainly include wet flue gas desulfurization, dry sorbent injection, and spray dryer absorption; denitration technologies mainly include low nitrogen oxide combustion technology, selective catalytic reduction (SCR), and selective noncatalytic reduction; dust removal technologies mainly include electrostatic precipitators, bag filters, and ceramic filter tubes (CFTs). Combining different pollutant treatment technologies to achieve comprehensive flue gas purification not only increases the floor space but also increases equipment investment and operating costs.

The ceramic catalytic filter tubes (CCFTs) are made of dust removal filter tubes combined with denitration catalysts. The ceramic fiber filter tube can realize the integrated removal of high-temperature particulate matter,  $\text{NO}_x$ , and  $\text{SO}_x$ . The main structure of the CCFT is shown in Figure 1. The porous fiber structure of the CCFT can remove dust in the flue gas. At the same time, due to the action of the denitration catalyst and  $\text{NH}_3$ , the  $\text{NO}_x$  in the flue gas is selectively catalytically reduced to  $\text{N}_2$  and  $\text{H}_2\text{O}$ . By injecting the desulfurizer upstream,  $\text{SO}_x$  and  $\text{HCl}$  in

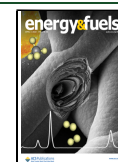
the flue gas can also be removed. Then, the incompletely reacted desulfurizer is removed through the filter tube and adsorbed on the outer surface of the filter tube to further remove the acid gas. The CCFT has the advantages of high-temperature resistance, corrosion resistance, high dust removal efficiency, comprehensive removal of multiple pollutants, low system energy consumption, and moderate economic cost.

Steffen Heidenreich<sup>2</sup> classified CFTs into high-density ceramics and low-density ceramics according to their density. High-density ceramics are made of silicon carbide,<sup>3</sup> alumina, and cordierite. The high-density sintered ceramic tube is prepared by integral extrusion molding, high-temperature sintering, secondary coating, and secondary calcination processes. However, the ceramic tube has low porosity (<40%) and low axial strength. The product after sintering is brittle to break, and its size is limited. Low-density ceramics are made of aluminium silicate fibers. The low-density CFT has the characteristics of high strength, low pressure drop, and a high porosity (>80%). The low-density CFTs are promising for continuous industrialized production. Some scholars have studied ceramic catalytic filter elements in the industrial applications of flue gas purification.<sup>4,5</sup>

Received: December 22, 2021

Revised: March 5, 2022

Published: March 21, 2022



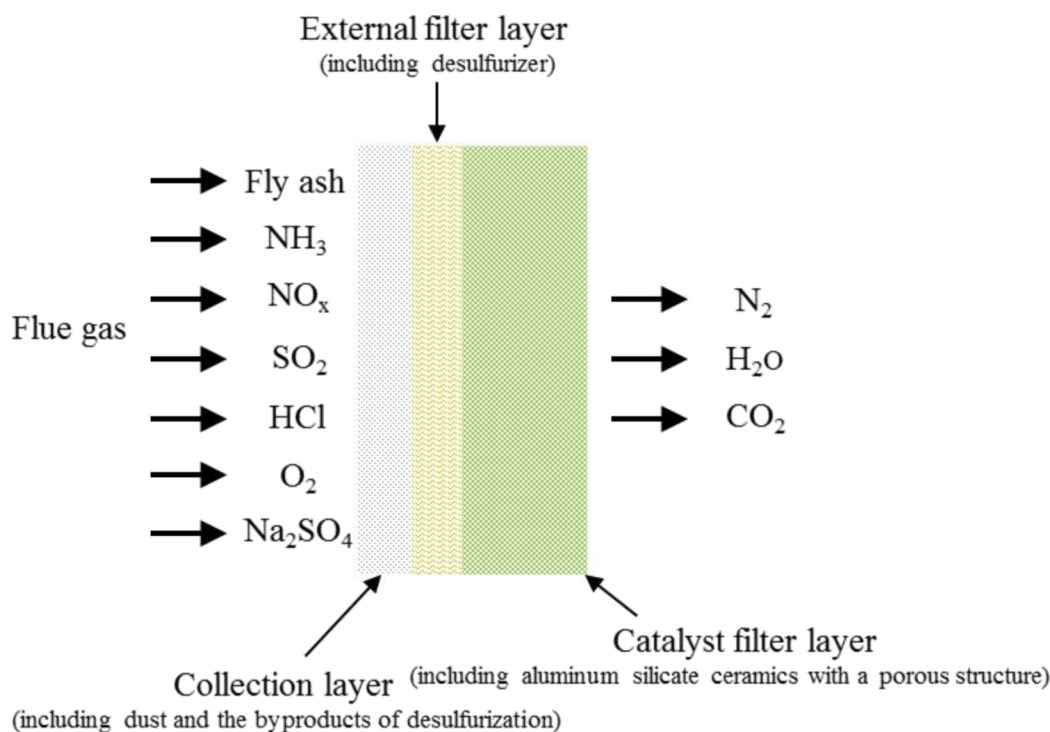


Figure 1. Main structure of the ceramic catalytic filter tube.

Walberer et al.<sup>4</sup> used five modified catalysts and precoated  $\text{Ca}(\text{OH})_2$  on the outside of the SiC CFTs to study the removal of multiple pollutants at low temperatures (150–200 °C). Tan et al.<sup>5</sup> used the CCFT made of aluminium silicate fibers and used  $\text{NaHCO}_3$  as a desulfurizer to remove  $\text{SO}_2$  and  $\text{HCl}$ .

A catalyst is the key factor for SCR to affect the denitration efficiency. At present, studies have shown that  $\text{V}_2\text{O}_5\text{--}\text{WO}_3(\text{MoO}_3)/\text{TiO}_2$  catalysts are widely used in denitration systems.<sup>6–8</sup> The denitration efficiency is high, and the SCR system operates stably. According to the type of the catalyst, the SCR catalyst system is mainly divided into three kinds: V–Ti oxide, V–W–Ti oxide, and V–Mo–Ti oxide. The catalyst system generally uses  $\text{V}_2\text{O}_5$  as the active ingredient,  $\text{WO}_3$  or  $\text{MoO}_3$  as the auxiliary agent, and  $\text{TiO}_2$  as the carrier.<sup>6</sup>

Numerous studies on the denitration efficiency of catalysts, catalyst loadings, and ceramic types have been carried out. Research on the effect of different types of filter tubes on the denitration efficiency has been carried out for the catalytic system of V–Ti oxide.<sup>9–11</sup> Saracco and Specchia<sup>9</sup> prepared  $\text{V}_2\text{O}_5\text{--}\text{TiO}_2$  alumina fiber filters to study the effect of the amount of catalyst loading on the removal of pollutants. The desulfurization efficiency was 70–80%, and the denitration efficiency was 90%. The dust removal efficiency was 99%. Kamble et al.<sup>10</sup> studied  $\text{V}_2\text{O}_5\text{--}\text{TiO}_2$  supported by aluminum silicate water filter tubes, and the  $\text{NO}_x$  reduction rate of the catalyst synthesized under the optimal conditions was greater than 97%. Choi et al.<sup>11</sup> studied the effect of adding Pt on the catalytic activity of the filter tube at low temperatures. The catalytic filter with Pt added shifted the optimal working temperature from 280–330 to 180–230 °C.

The effects of catalysts, catalyst loadings, and ceramic types have been investigated in laboratory-scale denitration experiments for the catalytic system of V–W–Ti oxide.<sup>12–18</sup> Hackel et al.<sup>12</sup> conducted denitration experiments in the SiC filter tubes covered with a mullite membrane. Heidenreich et al.<sup>13,14</sup>

intercepted a section of the catalytic filter tube and injected  $\text{NaHCO}_3$  into the gas upstream of the filter chamber. They studied the catalytic performance of the filter element in a laboratory-scale atmospheric reactor. Studies showed that when the  $\text{NO}$  inlet concentration was 500 ppmv and the reaction temperature was 300 °C, the denitration efficiency reached up to 98%. The removal rate of  $\text{SO}_x$  was 99%, and the dust removal efficiency was 99.9997%. In addition, Zürcher et al.<sup>15</sup> also studied a ceramic sponge impregnated with a catalyst into a SiC CFT. The study showed that the denitration efficiency was 100% in the range of 260–340 °C, and the denitration efficiency was the highest at 300 °C. Wang et al.<sup>16</sup> prepared  $\text{V}_2\text{O}_5\text{--}\text{WO}_3\text{--}\text{TiO}_2$  catalytic filter for particle separation and denitration. They investigated the effect of the amount of catalyst loading on the denitration efficiency. Kim et al.<sup>17</sup> used a  $\text{TiO}_2$  particle solution to coat the pore surface of the SiC filter element and measured the additional effect of Pt on a catalytic filter based on  $\text{V}_2\text{O}_5\text{--}\text{WO}_3\text{--}\text{TiO}_2$ . Fino et al.<sup>18</sup> prepared five SCR catalysts and found that the combination of  $\text{MnO}_x\text{--}\text{CeO}_2$  and  $\text{V}_2\text{O}_5\text{--}\text{WO}_3\text{--}\text{TiO}_2$  catalysts can achieve the highest  $\text{NO}_x$  and volatile organic compounds removal efficiency.

For a catalytic system of V–Mo–Ti oxide, the temperature range of the denitration reaction, the comparison with the V–Mo–Ti oxide, and the activity of the catalyst after poisoning have been explored.<sup>6–8,19–21</sup> Lietti et al.<sup>6</sup> found that the  $\text{V}_2\text{O}_5\text{--}\text{MoO}_3/\text{TiO}_2$  catalyst showed higher activity than the  $\text{V}_2\text{O}_5\text{--}\text{WO}_3/\text{TiO}_2$  catalyst. However,  $\text{MoO}_3$  reacts to form  $\text{N}_2\text{O}$  at high temperatures (>377 °C), and the denitration efficiency decreases significantly. Casagrande et al.<sup>8</sup> found that the ternary catalyst  $\text{V}_2\text{O}_5\text{--}\text{MoO}_3/\text{TiO}_2$  was more active in the denitration reaction than the binary catalyst  $\text{V}_2\text{O}_5/\text{TiO}_2$  or  $\text{MoO}_3/\text{TiO}_2$ .  $\text{MoO}_3$  expanded the temperature range of the denitration reaction, and the denitration reaction temperature was lower. Peng et al.<sup>19</sup> and Kobayashi et al.<sup>20</sup> found that SCR catalysts using  $\text{MoO}_3$  showed better resistance to As and  $\text{SO}_2$  poisoning

effects compared to  $\text{WO}_3$ .<sup>19,20</sup> Thus, the  $\text{V}_2\text{O}_5\text{--MoO}_3/\text{TiO}_2$  catalyst has higher catalytic activity than the  $\text{V}_2\text{O}_5\text{--WO}_3/\text{TiO}_2$  catalyst.

In this study, we used a vacuum centrifugal suction filtration technology to develop ceramic fiber filter tubes with high strength and low pressure drop. The V, Mo nanocatalyst slurry with metatitanic acid as the carrier precursor was implanted into the ceramic fiber filter tube. By injecting  $\text{NaHCO}_3$  upstream, the desulfurization, denitrification, and dust removal characteristics of the CCFT from 180 to 330 °C were investigated. We designed a pilot-scale experiment system. The inlet gas ( $\text{SO}_2$ ,  $\text{NO}$ , and  $\text{H}_2\text{O}$ ) was introduced into the flue, and  $\text{NaHCO}_3$  was injected into the flue in the form of a mixture of air and powder under the action of a feeder and an air compressor. The effects of the  $\text{NO}_x$  concentration, the ammonia–nitrogen ratio (NSR), the filtration velocity in the CFT, and the reaction temperature on the separate denitrification process were investigated. In addition, the effects of the filtration velocity, the reaction temperature, and the sodium–sulfur ratio (SSR) in the CFT on the simultaneous desulfurization and denitrification process were also studied.

## 2. EXPERIMENTAL SECTION

**2.1. Materials.** The CCFTs (Jiangsu Saitu New Material Technology Co., Ltd.) use fibers as raw materials and adopt a vacuum centrifugal suction filtration process. At the same time, the slurry feeding speed, vacuum degree, and centrifugal speed are adjusted to control the wall thickness deviation of the CCFT within 5%. The strength of the CCFT is greater than 1 MPa, and the porosity is greater than 80%. The nano-oxide liquid phase synthesis technology is to transform from V and Mo salt to a nano-oxide. The nano-oxide is oriented and loaded on the metatitanic acid carrier. The above-mentioned nanocatalyst slurry is a raw material, and the nanocatalyst is uniformly implanted into the ceramic fiber filter tube through the vapor deposition effect of a vacuum pump. The CCFTs are shown in Figure 2.

**2.2. Experimental Equipment and Conditions.** **2.2.1. Experimental Equipment.** The schematic diagram of the experimental system is shown in Figure 3. The lengths of the flues are shown in millimeters. The main components of the system included an industrial air heater, a  $\text{NO}$  and  $\text{SO}_2$  gas delivery device, a  $\text{NaHCO}_3$  powder feeding device, a ceramic multitube dust collector, and an induced draft fan. The inner diameter of the pipe is 120 mm. The hot air blower is used to generate hot air at a set temperature, and the flow rate is adjustable. The  $\text{NO}$  and  $\text{SO}_2$  gas delivery device controls the initial  $\text{NO}$  concentration and  $\text{SO}_2$  concentration. After various gases are uniformly mixed,  $\text{NH}_3$  is introduced for the catalytic reduction reaction. Three mass flow controllers (MFCs) are used to control the flow rate of gases.  $\text{NO}$  is stored in cylinders as a mixture containing 8%  $\text{NO}$  and 92%  $\text{N}_2$ . The gas concentration of  $\text{SO}_2$  and  $\text{NH}_3$  is 99.999%. A steam generator (24/48 kW, Shangrao Jiangxin Boiler Co., Ltd.) is used to generate water vapor in the flue gas. A vortex flowmeter (SV21 and SENER) monitors the mass flow rate of water vapor.  $\text{NaHCO}_3$  is injected into the flue in the form of a mixture of air and powder under the action of a feeder and an air compressor. The particle size of  $\text{NaHCO}_3$  powder (Weifang Jiejia Chemical Co., Ltd.) was measured with a laser particle size analyzer (Beckman Coulter LS13320, Coulter, USA). The average particle size of  $\text{NaHCO}_3$  was 9.053  $\mu\text{m}$ , and the median particle size was 5.894  $\mu\text{m}$ . Two gas detection points were arranged, and the concentrations of pollutants were measured using a flue gas analyzer (Testo 350) with a resolution of 1 ppm. The pressure measuring points and temperature measuring points were arranged at the inlet and outlet of the dust collector. The differential pressure meter (Testo 512) measured the pipe pressure and gas flow rate. A K-type thermocouple was used to measure the temperature of flue gas. An automatic flue gas sampling tester (3012H, Qingdao Laoshan Applied Technology Research Institute) was used for dust detection. Finally, the flue gas



Figure 2. Ceramic catalytic filter tubes.

was filtered using a ceramic multitube dust collector and then discharged by the induced draft fan.

Twelve ceramic fiber filter tubes were installed in the filter tube dust collector. The size of the filter tube installation plane was 1020 mm  $\times$  800 mm. The distance between the filter tube installation plane and hopper was 2000 mm. The CCFT was 2000 mm long, with an outer diameter of 200 mm and an inner diameter of 150 mm. The gas storage tank had a size of  $\Phi 121$  mm  $\times$  600 mm and a volume of 0.00678  $\text{m}^3$ . The air supply pressure was 0.6–0.7 MPa. Three DMF-MF40 electromagnetic pulse valves were used. Each valve controlled the back-blowing and dust removal of the four filter pipes in a single row. The dust collector was covered with an aluminum silicate material with a thickness of 150 mm to prevent heat loss.

**2.2.2. Characterization Method.** The Brunauer–Emmett–Teller (BET) surface area and pore size distribution of the CCFT were measured using a Micromeritics ASAP 2460 nitrogen adsorption device. The degassing temperature was 200 °C, and the degassing time was 8 h. A Zeiss Sigma 300 scanning electron microscope was used to observe the morphology of the CCFT by scanning electron microscopy (SEM). The surface binding and element morphology were analyzed by X-ray photoelectron spectroscopy (XPS) using a Thermo Scientific K-alpha ray photoelectron spectrometer, with a surface excitation at 1486.6 eV using an Al K-alpha ray source. The survey and high-resolution spectra of  $\text{V}_{2p}$ ,  $\text{Mo}_{3d}$ , and  $\text{O}_{1s}$  were collected and calibrated with a binding energy of  $\text{C}_{1s}$  of 284.68 eV. To further determine the composition of the CCFT, X-ray fluorescence (XRF) analysis was performed using Shimadzu XRF-1800. The thermal weight loss behavior of the CCFT was analyzed by thermogravimetric analysis (TGA) using a NETZSCH STA449F3. The detailed testing conditions are as follows: the mass of the sample was 7.45 mg, the heating rate was 20 °C/min, and the sample was heated from 50 to 1000 °C under a  $\text{N}_2$  atmosphere.

**2.2.3. Experimental Procedures.** The industrial air heater was turned on to set the heating temperature to heat the inlet air. The

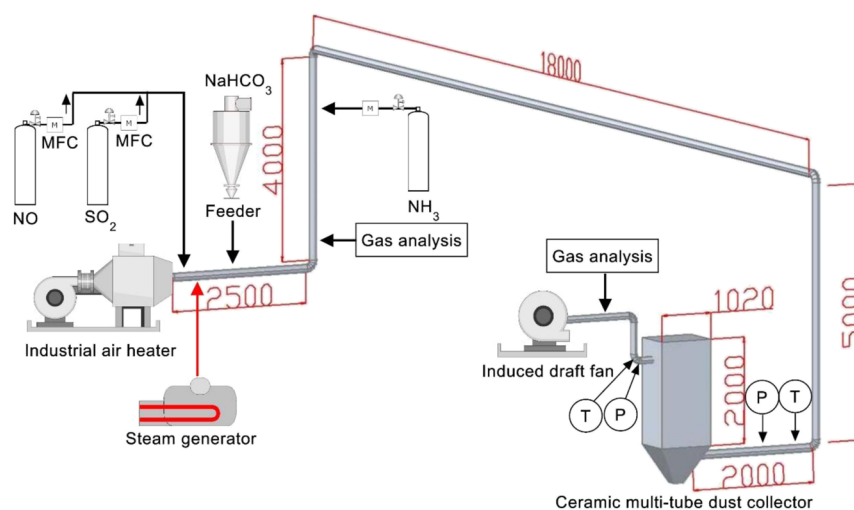


Figure 3. Schematic diagram of the experimental system.

Table 1. Experimental Conditions

	variable	the average temperature in the dust collector (°C)	inlet NO <sub>x</sub> concentration (mg/Nm <sup>3</sup> )	inlet SO <sub>2</sub> concentration (mg/Nm <sup>3</sup> )	the filtration velocity (m/min)	NSR	SSR
separate denitration	the reaction temperature	180, 230, 280, 330	150–450	0	0.6–1.2	1.0	
	the inlet NO <sub>x</sub> concentration	180–330	150, 250, 350, 450	0	0.6–1.2	1.0	
	the filtration velocity	230–330	350	0	0.6, 0.8, 1.0, 1.2	1.0	
	NSR	230–330	350	0	0.8	0.7, 1.0, 1.2, 1.5	
simultaneous desulfurization and denitration	the filtration velocity	230–330	350	150	0.8, 1.0	1.0	1.0–2.0
	the reaction temperature	230, 280, 330	350	150	0.8–1.0	1.0	1.0–2.0
	SSR	230–330	350	150	0.8–1.0	1.0	1.0, 1.5, 2.0

induced draft fan was turned on. The CCFT was preheated for 72 h to activate the denitration characteristics at 200 °C. The airflow velocity was measured using a differential pressure meter. The baffle of the industrial air heater and the power of the induced draft fan were adjusted to make the gas flow rate meet the experimental requirements. The temperature of the flue gas was measured using a thermocouple. A silicone tube and a differential pressure meter were used to measure the pressure drop between the inlet and outlet of the dust collector. When the experimental system was stabilized, the NO, SO<sub>2</sub>, and NH<sub>3</sub> gas bottles were opened and controlled using the MFCs. The NO<sub>x</sub> and SO<sub>2</sub> concentrations were measured using a Testo flue gas analyzer. The steam generator was turned on, and the water vapor in the flue gas was 15 vol %. The experimental conditions are shown in Table 1. The reaction temperature was the average of the inlet temperature and outlet temperature of the dust collector. The outlet pollutants of the dust collector were measured to calculate the desulfurization and denitrification efficiency. Taking NO<sub>x</sub> as an example, the NO<sub>x</sub> removal efficiency was calculated as follows

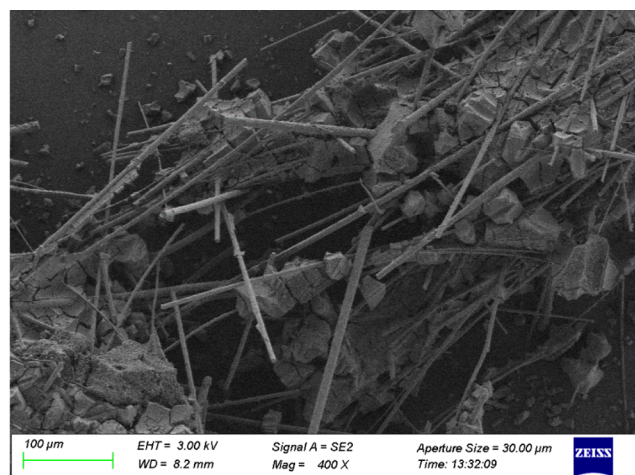
$$\text{NO}_x \text{ removal (\%)} = \frac{\text{NO}_{x,\text{in}} - \text{NO}_{x,\text{out}}}{\text{NO}_{x,\text{in}}} \times 100\% \quad (1)$$

### 3. RESULTS AND DISCUSSION

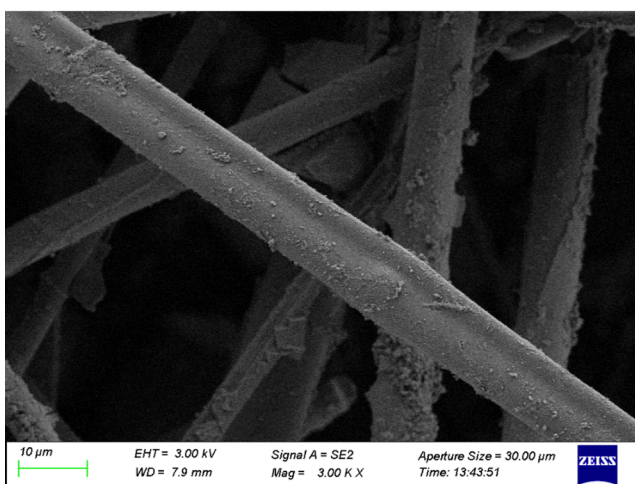
**3.1. Results of Characterization.** Figure 4 presents the SEM images of the CCFT. The aluminum silicate fiber is a low-density ceramic material. Due to its loose structure, the ceramic

filter element formed from the fibers has a higher porosity and lower resistance. At the same time, the mechanical strength of the ceramic filter element is low, and there is a risk of fracture. The catalyst was supported on the fiber, which increased the BET surface area of the CCFT. Table 2 lists the BET results of the CCFT. The BET surface area, micropore volume, and average pore diameter are 64.72 m<sup>2</sup>/g, 0.0025 cm<sup>3</sup>/g, and 8.79 nm, respectively.

Figure 5 shows the TGA results of the CCFT. The weight loss below 120 °C was obvious, with a weight loss rate of up to 6.81%. This weight loss was due to the evaporation of water. However, the weight loss is not obvious at the temperature between 120 and 1000 °C, and the weight loss rate was 1.73%. This shows that the CCFT has thermal stability under the experimental conditions. Figure 6 shows the XPS results of the CCFT. There were three distinct peaks at 516.3, 525.2, and 232.6 eV, corresponding to V<sub>2p</sub>, Mo<sub>3d</sub>, and O<sub>1s</sub>, respectively. Table 3 shows the XRF results of the CCFT. XRF analysis showed that the main components in the CCFT were SiO<sub>2</sub>, TiO<sub>2</sub>, and Al<sub>2</sub>O<sub>3</sub>. The main component of the CCFT was aluminum silicate. The mass fraction of SiO<sub>2</sub> and Al<sub>2</sub>O<sub>3</sub> was 63.62 and 14.32%, respectively. The mass fraction of TiO<sub>2</sub> was 16.66%. This was because the catalyst slurry was formed by supporting the metatitanic acid carrier with nano-oxides. The active compo-



(a)



(b)

Figure 4. SEM images of the CCFT: (a)  $\times 400$  and (b)  $\times 3000$ .

Table 2. Physical Properties of the CCFT

BET surface area (m <sup>2</sup> /g)	micropore volume (cm <sup>3</sup> /g)	average pore diameter (nm)
64.72	0.0025	8.79

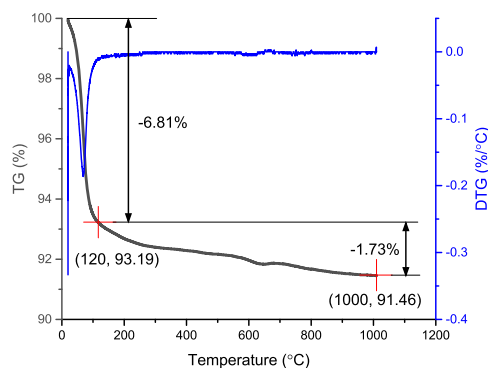
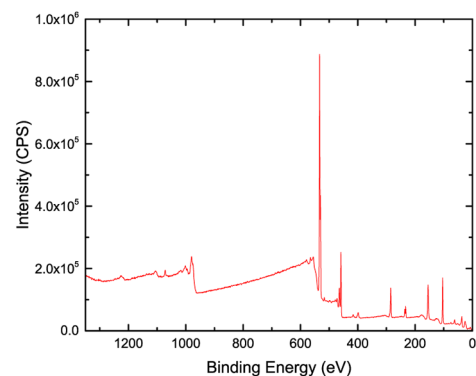


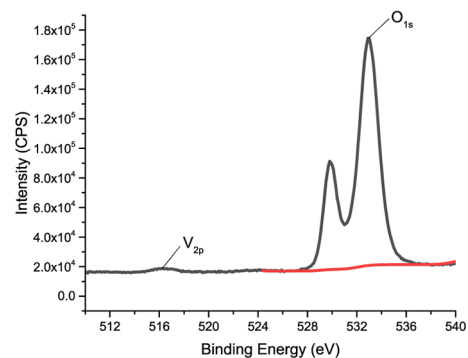
Figure 5. TGA results of the CCFT.

nents were MoO<sub>3</sub> and V<sub>2</sub>O<sub>5</sub>, and the mass fraction was 1.84 and 1.09%, respectively.

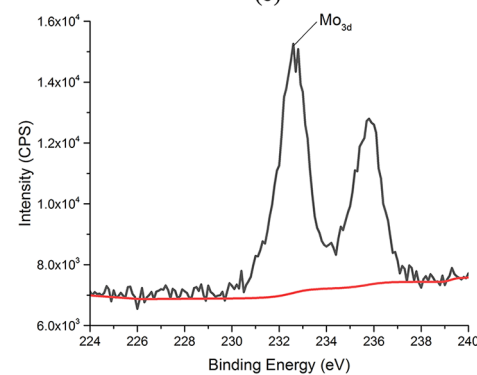
**3.2. Pressure Drop and Dust Removal Efficiency of the Dust Collector.** Fly ash with a mass flow rate of 30 g/Nm<sup>3</sup> and



(a)



(b)



(c)

Figure 6. XPS results of the CCFT: (a) full XPS spectrum, (b) oxygen and vanadium, and (c) molybdenum.

Table 3. XRF Results of the CCFT

composition	mass fraction (%)
SiO <sub>2</sub>	63.62
TiO <sub>2</sub>	16.66
Al <sub>2</sub> O <sub>3</sub>	14.32
MoO <sub>3</sub>	1.84
V <sub>2</sub> O <sub>5</sub>	1.09
SO <sub>3</sub>	0.77
ZrO <sub>2</sub>	0.55
Na <sub>2</sub> O	0.50
CaO	0.27
K <sub>2</sub> O	0.12
P <sub>2</sub> O <sub>5</sub>	0.047

an average particle size of 12.51  $\mu\text{m}$  was introduced into the flue. An automatic flue gas sampling tester (3012H, Qingdao

Laoshan Applied Technology Research Institute) was used for dust detection at the outlet of the dust collector. The experimental results found that the dust removal efficiency of the CFT was 99.90%. The pressure drop of the dust collector is shown in Table 4. As the temperature increased, the pressure

**Table 4. Pressure Drop of the Dust Collector**

the average temperature in the dust collector (°C)	the filtration velocity (m/min)	the pressure drop of the dust collector (Pa)
230	0.8	680
	1.0	890
280	0.8	645
	1.0	870
330	0.8	635
	1.0	840

drop of the dust collector decreased. As the filtration velocity increased, the pressure drop of the dust collector increased. When the filter velocity was 1.0 m/min at 230 °C, the maximum pressure drop of the dust collector was 890 Pa. When the filter velocity was 0.8 m/min at 330 °C, the minimum pressure drop of the dust collector was 635 Pa.

**3.3. Impact of the Reaction Temperature on the Denitration Efficiency.** When the filtration velocity in the filter tube was 0.6, 0.8, 1.0, and 1.2 m/min, the average temperature inside the dust collector was adjusted to 180, 230, 280, and 330 °C, respectively. The NSR was set to be 1. Figure 7 shows the denitration efficiencies of the filter tube at different reaction temperatures (the average temperature in the dust

collector) and filtration velocities. At the same filtration velocity, as the reaction temperature increased, the denitration efficiency first increased and then remained unchanged. The relationship between the reaction temperature and denitration efficiency exhibited two-stage characteristics. The first stage occurred at the reaction temperature of 180–280 °C, and these two parameters were positively correlated with a linear relationship. The second stage occurred at the reaction temperature of 280–330 °C, and the denitration efficiency basically remained at a constant high value. These phenomena occurred because when the reaction temperature increased, the catalyst activity in the dust collector increased, leading to more intensive reactions and higher denitration efficiency. When the filtration velocity increased, the denitration efficiency decreased. In the second stage (280–330 °C), the denitration efficiency increased with the reaction temperature. According to the literature,<sup>4,5</sup> when the reaction temperature was 180 °C, the denitration efficiency reached 38%. When the reaction temperature was 250–350 °C, the denitration efficiency reached the highest level, which was greater than 90%. The experimental results obtained in this study are consistent with these results. Therefore, when the reaction temperature was set in the range of 280–330 °C, the denitration efficiency was high.

**3.4. Impact of the Inlet NO<sub>x</sub> Concentration on the Denitration Efficiency.** When the average temperature inside the dust collector was 180, 230, 280, and 330 °C, the inlet NO<sub>x</sub> concentration was adjusted to 150, 250, 350, and 450 mg/Nm<sup>3</sup>, respectively. The NSR was set to be 1. Figure 8 shows the denitration efficiencies of the filter tube at different NO<sub>x</sub>

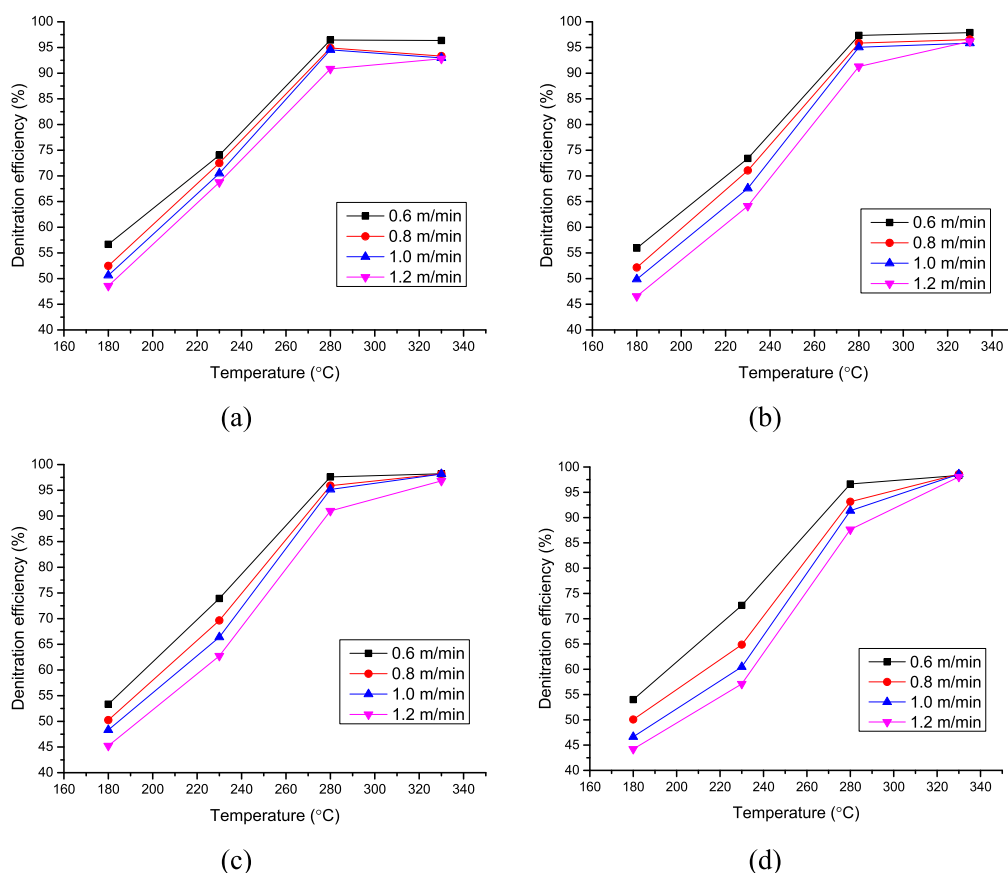


**Figure 7.** Denitration efficiencies of the filter tube at different reaction temperatures and filtration velocities [inlet NO<sub>x</sub> concentration: (a) 150; (b) 250; (c) 350; (d) 450 mg/Nm<sup>3</sup>].

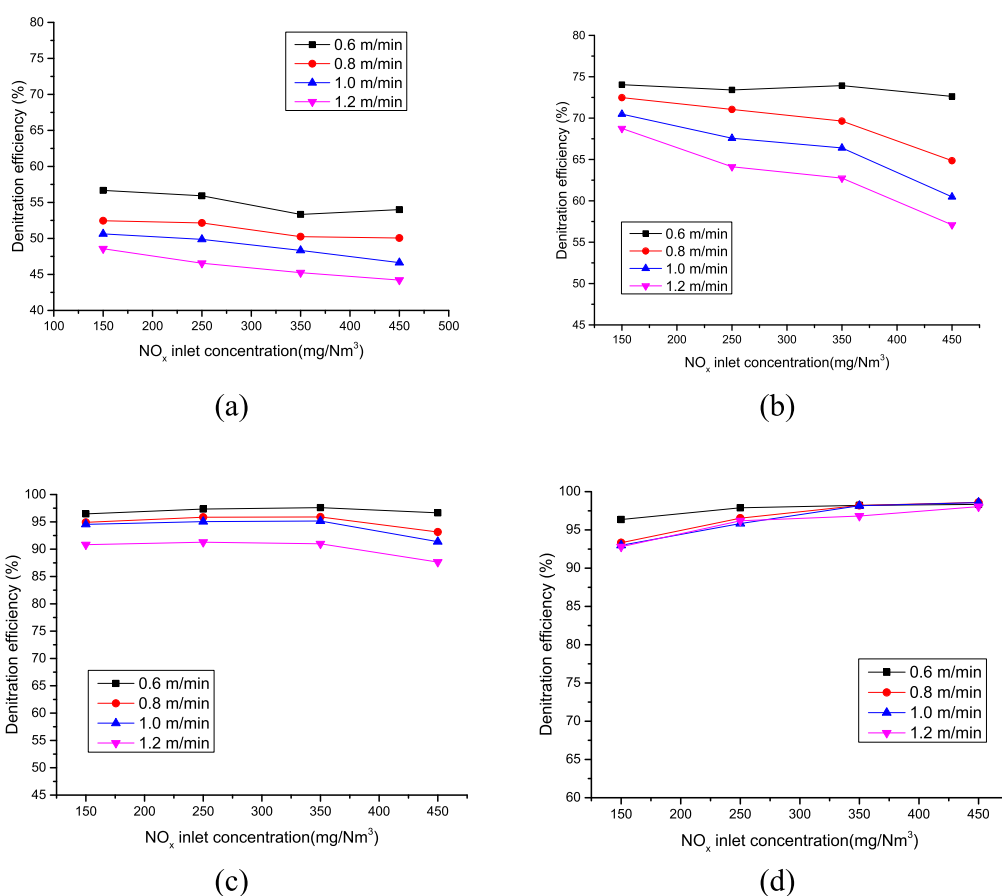


**Figure 8.** Denitration efficiencies of the filter tube at different  $\text{NO}_x$  concentrations and filtration velocities [reaction temperature: (a) 180; (b) 230; (c) 280; (d) 330 °C].

concentrations and filtration velocities. At the same temperature, the denitration efficiency of the filter tube decreased with an increase in the inlet  $\text{NO}_x$  concentration. Particularly, when the inlet  $\text{NO}_x$  concentration was greater than  $350 \text{ mg/Nm}^3$ , the denitration efficiency decreased significantly. This can probably be attributed to the fact that when the  $\text{NO}_x$  concentration increased, the ammonia gas and nitrogen oxide were not mixed adequately, leading to the reduction in the denitration efficiency of the filter tube. As the filtration velocity increased, the reduction in the denitration efficiency became more prominent. However, with an increase in the reaction temperature, the impact of the inlet  $\text{NO}_x$  concentration on the denitration efficiency of the filter tube became less significant. At high reaction temperatures ( $\geq 280 \text{ °C}$ ), the impact was small. Therefore, combined with Section 3.3, the reduction in the denitration efficiency caused by the inlet  $\text{NO}_x$  concentration could be compensated for by increasing the reaction temperature.

**3.5. Impact of the Filtration Velocity on the Denitration Efficiency.** When the average temperature inside the dust collector was 230, 280, and 330 °C, the filtration velocity of the ceramic fiber filter tube was adjusted to 0.6, 0.8, 1.0, and 1.2 m/min, respectively. Figure 9 shows the denitration efficiencies of the filter tube at different filtration velocities and reaction temperatures. At the same temperature, the denitration efficiency decreased significantly as the filtration velocity increased. This is because when the filtration velocity increased, the residence time of  $\text{NO}_x$  and  $\text{NH}_3$  in the system decreased, leading to a reduction in the contact time between the flue gas

and the catalyst. With an increase of the inlet  $\text{NO}_x$  concentration, the impact of the filtration velocity became more significant, resulting in a significant reduction in the denitration efficiency of the filter tube. This is because when the filtration velocity was high, the mixing of  $\text{NO}_x$  and  $\text{NH}_3$  was inadequate, which resulted in a decrease in the denitration efficiency of the filter tube. When the reaction temperature increased, the effect of the filtration velocity became weaker. When the reaction temperature was 330 °C, the effect of filtration velocity was negligible. The filtration velocity should be set in the range of 0.6–0.8 m/min to achieve high denitration efficiency.

At the reaction temperature of 180 °C, the highest denitration efficiency was 56.67% when the inlet  $\text{NO}_x$  concentration and the filtration velocity were  $150 \text{ mg/Nm}^3$  and 0.6 m/min, respectively. At the reaction temperature of 230 °C, the highest denitration efficiency was 73.93% when the inlet  $\text{NO}_x$  concentration and the filtration velocity were  $350 \text{ mg/Nm}^3$  and 0.6 m/min, respectively. At the reaction temperature of 280 °C, the highest denitration efficiency was 97.60% when the inlet  $\text{NO}_x$  concentration and the filtration velocity were  $350 \text{ mg/Nm}^3$  and 0.6 m/min, respectively. At the reaction temperature of 330 °C, the highest denitration efficiency was 98.59% when the inlet  $\text{NO}_x$  concentration and the filtration velocity were  $450 \text{ mg/Nm}^3$  and 0.8 m/min, respectively. At low reaction temperatures ( $\leq 230 \text{ °C}$ ), the effect of the inlet  $\text{NO}_x$  concentration was small as the filtration rate decreased. With a decrease in the reaction temperature, the catalyst activity and the denitration reaction rate decreased. When the filtration velocity decreased, the

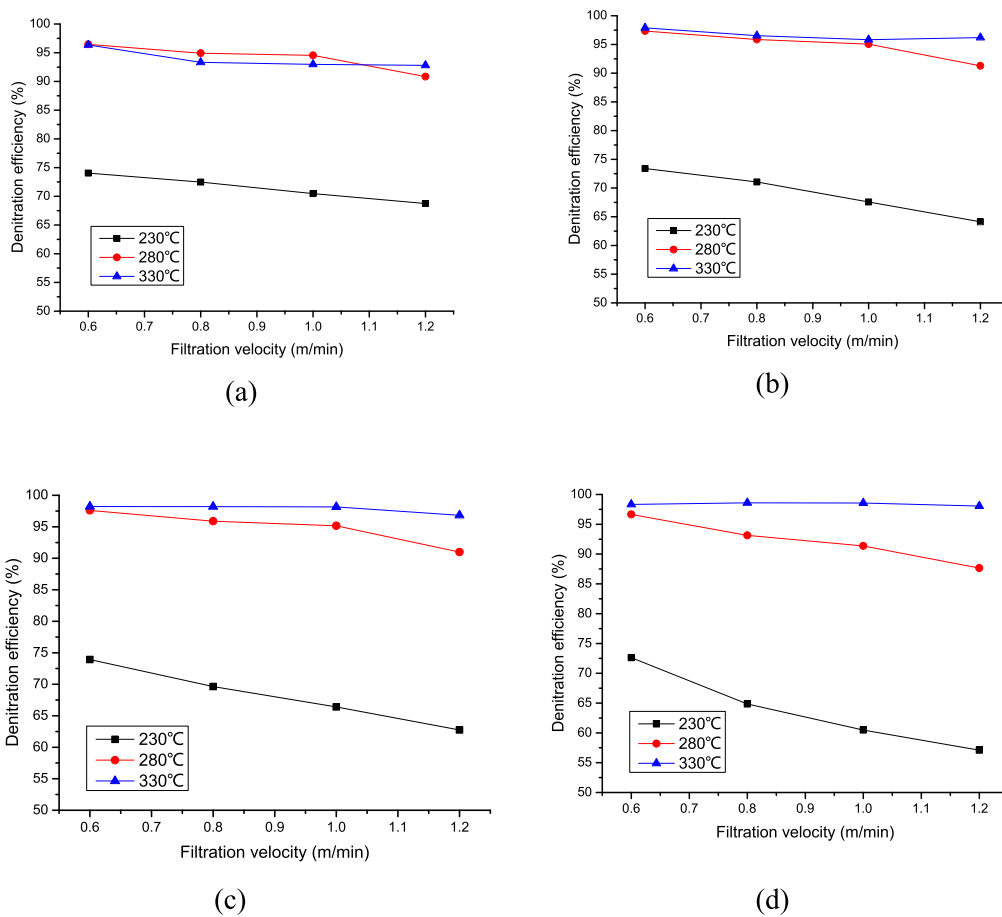


**Figure 9.** Denitration efficiencies of the filter tube at different filtration velocities and reaction temperatures [inlet NO<sub>x</sub> concentration: (a) 150; (b) 250; (c) 150; (d) 450 mg/Nm<sup>3</sup>].

contact time between the flue gas and the catalyst increased, and the denitration efficiency increased. Under the combined effect of the reaction temperature and filtration velocity, the inlet NO<sub>x</sub> concentration had little effect on the denitration efficiency. At high reaction temperatures ( $\geq 280$  °C), the inlet NO<sub>x</sub> concentration and filtration velocity had little effect on the denitration efficiency, as shown in Figures 8 and 9.

Therefore, at the reaction temperature of 180 °C, the optimal operating conditions were that the inlet NO<sub>x</sub> concentration was 150–350 mg/Nm<sup>3</sup> and the filtration velocity was 0.6–0.8 m/min. At the reaction temperature of 230 °C, the optimal operating conditions were that the inlet NO<sub>x</sub> concentration was 150–350 mg/Nm<sup>3</sup> and the filtration velocity was 0.6–0.8 m/min. At the reaction temperature of 280 °C, the optimal operating conditions were that the inlet NO<sub>x</sub> concentration was 150–350 mg/Nm<sup>3</sup> and the filtration velocity was 0.6–1.0 m/min. At the reaction temperature of 180 °C, the optimal operating conditions were that the inlet NO<sub>x</sub> concentration was 150–450 mg/Nm<sup>3</sup>, and the filtration velocity was 0.6–1.2 m/min.

### 3.6. Impact of the NSR on the Denitration Efficiency.

Figure 10 shows the denitration efficiencies at different NSRs and reaction temperatures. The NO<sub>x</sub> inlet concentration was 350 mg/Nm<sup>3</sup>, and the filtration velocity was 0.8 m/min. The experimental results showed that when the NSR increased, the denitrification efficiency increased. At 230 °C, the denitration efficiency at a NSR of 0.7 was 62.22%. When the NSR was 1.5, the denitration efficiency was the highest, which was 75.53%. At

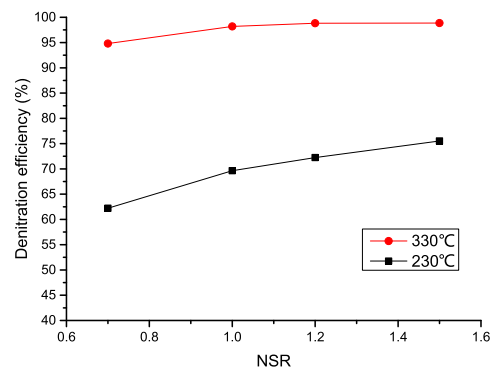


**Figure 10.** Denitration efficiencies at different NSRs and reaction temperatures.

330 °C, the denitration efficiency at a NSR of 0.7 was 94.81%. When the NSR was 1.5, the denitration efficiency was the highest, which was 98.86%. At low temperatures, the NSR had a greater impact on the denitrification efficiency.

**3.7. Effect of Different Filtration Speeds on the Simultaneous Desulfurization and Denitrification Efficiency.** When the average temperatures inside the dust collector were 230, 280, and 330 °C, the filtration velocity of the ceramic fiber filter tube was adjusted to 0.8 and 1.0 m/min, and the SO<sub>2</sub> and NO<sub>x</sub> inlet concentrations were, respectively, 150 and 350 mg/Nm<sup>3</sup>. The NSR and SSR were set to be 1. Figures 11 and 12 show the denitration and desulfurization efficiencies at different

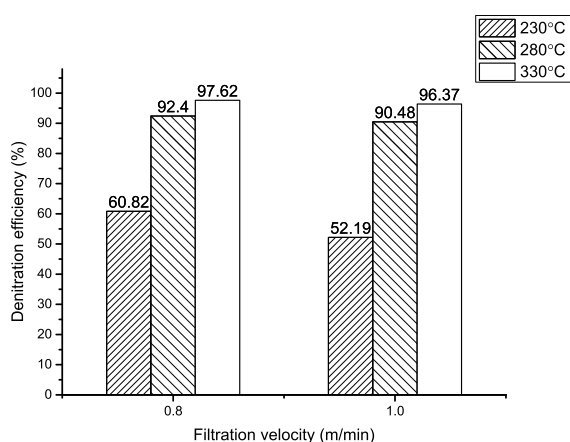


**Figure 11.** Denitrification efficiencies at different filtration velocities and reaction temperatures.

filtration velocities and reaction temperatures. At 230 °C, the highest denitrification efficiency was 60.82%; at 280 °C, the highest denitrification efficiency was 92.40%; at 330 °C, the highest denitrification efficiency was 97.62%. Figure 11 shows that at the same temperature, with the increasing filtration velocity, the denitrification efficiency decreased lightly. When the reaction temperature was 230 °C, with the increasing filtration velocity, the denitrification efficiency obviously decreased. Thus, when the reaction temperature was lower, the denitrification efficiency was more affected by the filtration velocity. Figure 12 shows that at the same temperature, with the increasing filtration velocity, the desulfurization efficiency decreased. Figure 12 shows that the desulfurization efficiency when the SSR = 2 was greater than the desulfurization efficiency when the SSR = 1. At 230 °C, the highest desulfurization efficiency was 88.38%; at 280 °C, the highest desulfurization efficiency was 94.23%; at 330 °C, the highest desulfurization efficiency was 94.23%.

The working conditions with high desulfurization and denitrification efficiency are as follows: the reaction temperature is 330 °C, the filtration velocity is 0.8 m/min, the SSR = 2. At 230 °C, the highest denitrification efficiency is 60.71%, and the highest desulfurization efficiency is 88.38%; at 280 °C, the highest denitrification efficiency is 92.40%, and the highest desulfurization efficiency is 94.23%; at 330 °C, the highest denitrification efficiency is 97.62%, and the highest desulfurization efficiency is 94.23%.

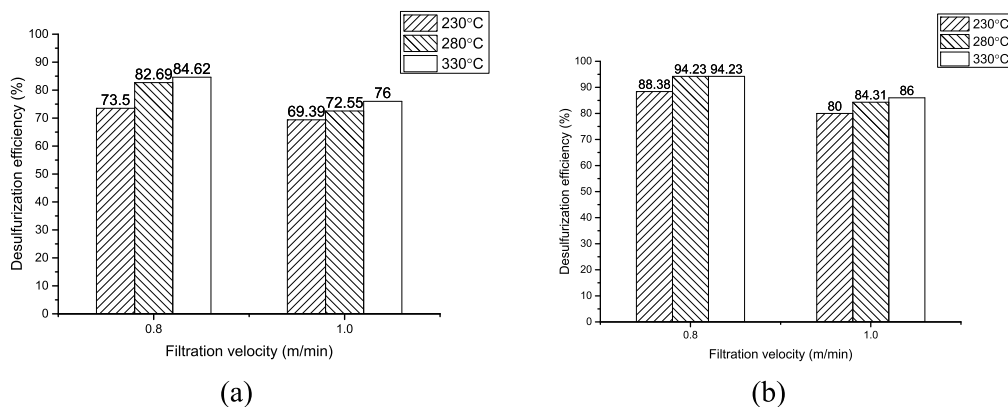


**Figure 12.** Desulfurization efficiencies at different filtration velocities and reaction temperatures [(a) SSR = 1; (b) SSR = 2].

**3.8. Effect of Different Reaction Temperatures on the Simultaneous Desulfurization and Denitrification Efficiency.** When the filtration speeds of the filter tube were 0.8 and 1.0 m/min, the reaction temperature was adjusted to 230, 280, and 330 °C, and the SO<sub>2</sub> and NO<sub>x</sub> inlet concentrations were set to be 150 mg/Nm<sup>3</sup> and 350 mg/Nm<sup>3</sup>, respectively. The NSR and SSR were set to be 1. Figures 13 and 14 show the denitrification

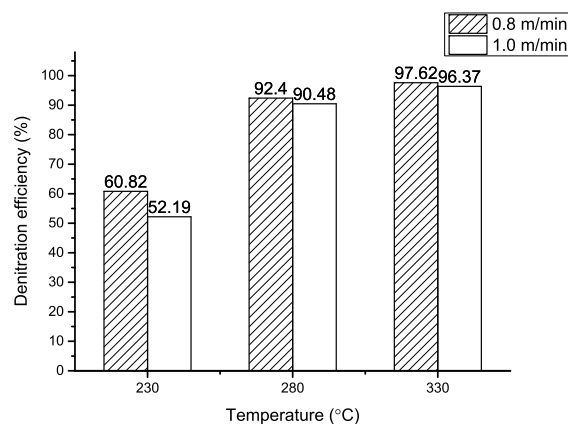


**Figure 13.** Denitrification efficiencies at different reaction temperatures and filtration velocities.

and desulfurization efficiencies at different reaction temperatures and filtration velocities. It can be seen in Figure 13 that at the same filtration velocity, as the reaction temperature increases, the denitrification efficiency gradually increases. When compared with a separate denitrification experiment, it is found that the denitrification efficiency of the simultaneous desulfurization and denitrification experiment is lower, indicating that SO<sub>2</sub> has an inhibitory effect on the denitrification reaction. This may be because SO<sub>2</sub>, NH<sub>3</sub>, and water vapor generate NH<sub>4</sub>HSO<sub>4</sub> at a low temperature. NH<sub>4</sub>HSO<sub>4</sub> will deactivate the catalyst at low temperatures (<280 °C) and affect the denitrification efficiency. At 330 °C, the denitrification efficiency was the highest, 97.62%. When the temperature was lower, the denitrification efficiency decreased more significantly.

SO<sub>2</sub> has an effect on the activity of the SCR catalyst. Under the conditions of 230 °C, a filtration speed of 0.8 m/min, and an inlet NO<sub>x</sub> concentration of 350 mg/Nm<sup>3</sup>, the stability test result is shown in Figure 15. The catalyst was tested for 6 h. The denitrification efficiency dropped slightly from 95.90 to 92.40% during the test. After turning off SO<sub>2</sub>, the denitrification efficiency

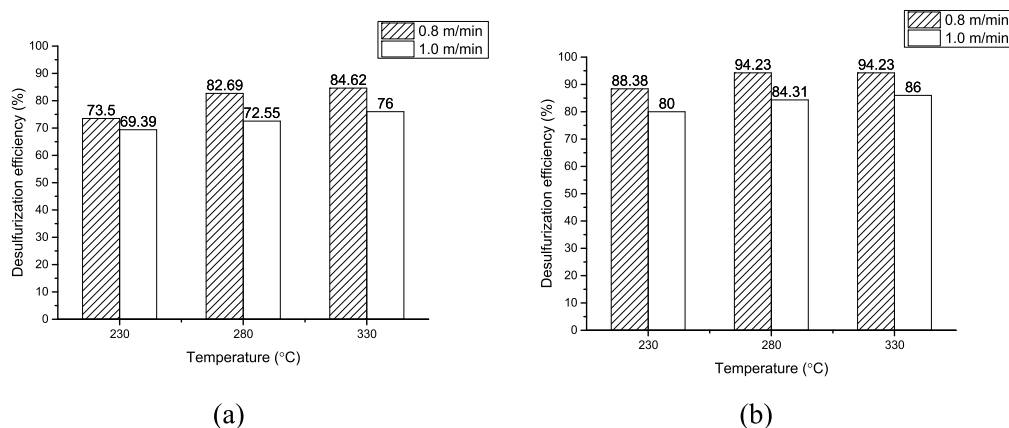


Figure 14. Desulfurization efficiencies at different reaction temperatures and filtration velocities [(a) SSR = 1; (b) SSR = 2].

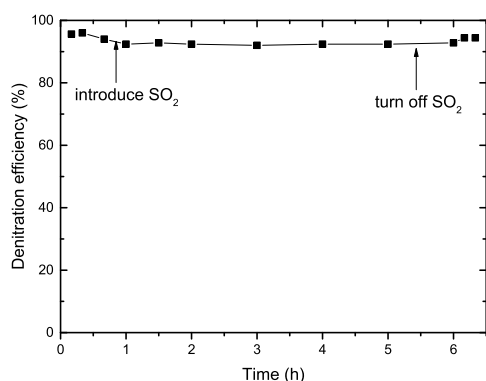


Figure 15. Catalyst stability test.

was restored to 94.40%. The denitration efficiencies of the catalyst after the stability test at different temperatures are shown in Table 5. The results showed that the catalyst exhibited good stability in the presence of SO<sub>2</sub>.

Table 5. Desulfurization Efficiency after Stability Test

the average temperature in the dust collector (°C)	the desulfurization efficiency without SO <sub>2</sub> (%)	the desulfurization efficiency with SO <sub>2</sub> (%)	the desulfurization efficiency after stability test (%)
230	69.64	60.82	64.49
280	95.90	92.40	94.40
330	98.19	97.62	98.02

It can be seen in Figure 14 that at the same filtration rate, as the reaction temperature increases, the desulfurization efficiency increases. This is because NaHCO<sub>3</sub> will decompose and release CO<sub>2</sub> at high temperatures (>210 °C), forming more micro-porous structures and providing more surface areas. Thus, NaHCO<sub>3</sub> is exposed more thoroughly to the flue gas, which is conducive to the progress of the desulfurization reaction. At the same time, Na<sub>2</sub>CO<sub>3</sub> produced by the pyrolysis of NaHCO<sub>3</sub> can continue to participate in the SO<sub>2</sub> removal reaction and help in the desulfurization reaction to proceed quickly and continuously. At 230 °C, the highest desulfurization efficiency is 88.38%; at 280 °C, the highest desulfurization efficiency is 94.23%; at 330 °C, the highest desulfurization efficiency is 94.23%.

**3.9. Effect of Different SSRs on the Simultaneous Desulfurization and Denitrification Efficiency.** When the

filtration velocities of the filter tube were 0.8 and 1.0 m/min, the average temperature inside the dust collector was adjusted to 230, 280, and 330 °C. The SSR was set to be 1, 1.5, and 2. Figure 16 shows the desulfurization efficiencies at different SSRs and reaction temperatures. It can be seen in Figure 16 that at the same reaction temperature, as the SSR increases, the desulfurization efficiency gradually increases. When the SSR increases, the concentration of the reactants increases, the number of activated molecules per unit volume increases, and the number of effective collisions per unit time increases. Therefore, the desulfurization efficiency increases. When the SSR is 2, the desulfurization efficiency is the highest.

#### 4. CONCLUSIONS

- (1) In this study, we used a vacuum centrifugal suction filtration technology to develop ceramic fiber filter tubes with a high strength and low pressure drop. The V, Mo nanocatalyst slurry with metatitanic acid as the carrier precursor was implanted into the ceramic fiber filter tube. By injecting NaHCO<sub>3</sub> upstream, the desulfurization, denitrification, and dust removal characteristics of the CCFT from 180 to 330 °C were investigated. BET, XPS, TGA, SEM, and XRF techniques were used to determine the pore structure and elemental analysis of the CCFT.
- (2) As the reaction temperature increased, the denitration efficiency first increased and then remained constant. The relationship between the reaction temperature and denitration efficiency exhibited two-stage characteristics. When the reaction temperature was set in the range of 280–330 °C, the denitration efficiency was highest. At 280 °C, the maximum efficiency was 97.60% when the inlet NO<sub>x</sub> concentration was 350 mg/Nm<sup>3</sup>, and the filtration velocity was 0.6 m/min. At 330 °C, the maximum efficiency was 98.59% when the inlet NO<sub>x</sub> concentration was 450 mg/Nm<sup>3</sup>, and the filtration velocity was 0.8 m/min. As the inlet NO<sub>x</sub> concentration increased, the denitration efficiency decreased. With the increasing filtration velocity, the denitration efficiency decreased significantly. When the filtration velocity was set in the range of 0.6–0.8 m/min, the denitration efficiency was higher.
- (3) When compared with the separate denitration experiment, it was found that the denitration efficiency of simultaneous desulfurization and denitration experiments was lower, indicating that SO<sub>2</sub> had an inhibitory effect on

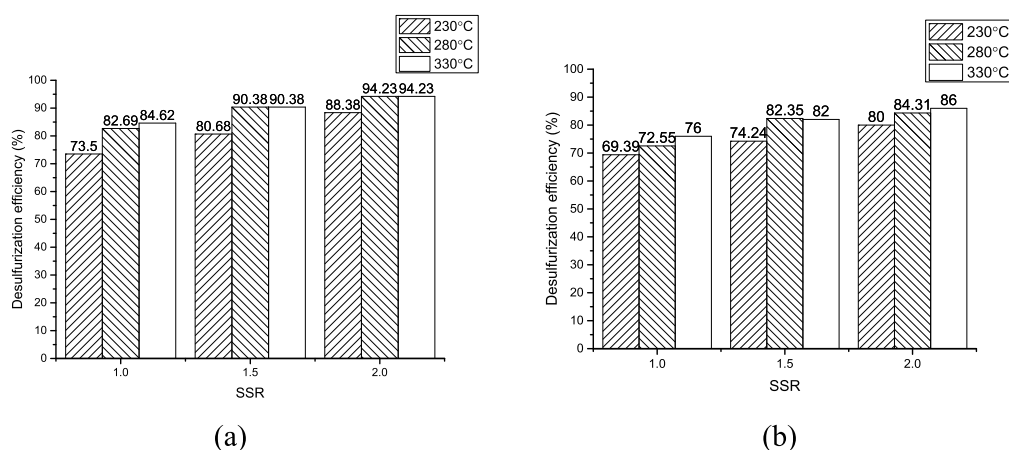


**Figure 16.** Desulfurization efficiencies at different SSRs and reaction temperatures [filtration velocity: (a) 0.8; (b) 1.0 m/min].

the denitration reaction. As the SSR increased, the desulfurization efficiency gradually increased. The working conditions with the highest desulfurization and denitrification efficiency in the experiment were as follows: the reaction temperature was 330 °C, the filtration velocity was 0.8 m/min, and the SSR was 2. At 230 °C, the highest denitration efficiency was 60.71%, and the highest desulfurization efficiency was 88.38%; at 280 °C, the highest denitration efficiency was 92.40%, and the highest desulfurization efficiency was 94.23%; at 330 °C, the highest denitration efficiency was 97.62%, and the highest desulfurization efficiency was 94.23%.

## AUTHOR INFORMATION

### Corresponding Author

**Hao Zhou** – State Key Laboratory of Clean Energy Utilization, Zhejiang University, Hangzhou 310027, China; [orcid.org/0000-0001-9779-7703](https://orcid.org/0000-0001-9779-7703); Phone: +86 571 87952598; Email: [zhouhao@zju.edu.cn](mailto:zhouhao@zju.edu.cn); Fax: +86 571 87951616

### Authors

**Yilin Song** – State Key Laboratory of Clean Energy Utilization, Zhejiang University, Hangzhou 310027, China

**Yize Zhang** – State Key Laboratory of Clean Energy Utilization, Zhejiang University, Hangzhou 310027, China

**Qiwei Wu** – State Key Laboratory of Clean Energy Utilization, Zhejiang University, Hangzhou 310027, China

**Di Kang** – Shanghai Electric Power Generation Environment Protection Engineering Company Ltd., Shanghai 201612, China

**Shiyi Guo** – Shanghai Electric Power Generation Environment Protection Engineering Company Ltd., Shanghai 201612, China

Complete contact information is available at: <https://pubs.acs.org/10.1021/acs.energyfuels.1c04342>

### Notes

The authors declare no competing financial interest. All data generated or analyzed during this study are included in this published article. If any researcher requests any data included in this study, it will be available upon request.

## ACKNOWLEDGMENTS

This work was supported by the National Science Fund for Distinguished Young Scholars (no. 51825605). The authors

thank Jiaqin Wang from Jiangsu Saitu New Material Technology Co., Ltd., who provided a brief introduction of CCFTs.

## REFERENCES

- (1) China Ison Track to Meet its Emissions Goals for 2020. <https://www.sciencedaily.com/releases/2019/10/191007113327.htm> (accessed October 10, 2021).
- (2) Heidenreich, S. Hot gas filtration - A review. *Fuel* **2013**, *104*, 83–94.
- (3) Heidenreich, S.; Haag, W.; Salinger, M. Next generation of ceramic hot gas filter with safety fuses integrated in venturi ejectors. *Fuel* **2013**, *108*, 19–23.
- (4) Walberer, J.; Giovanni, M.; Meiller, M.; Weih, C.; Hornung, A. Development and Tests of a Combined Filter for NO<sub>x</sub>, Particulates, and SO<sub>2</sub> Reduction. *Chem. Eng. Technol.* **2018**, *41*, 2150–2158.
- (5) Tan, Z.; Niu, G.; Qi, Q.; Zhou, M.; Wu, B.; Yao, W. Ultralow Emission of Dust, SO<sub>x</sub>, HCl, and NO<sub>x</sub> Using a Ceramic Catalytic Filter Tube. *Energy Fuels* **2020**, *34*, 4173–4182.
- (6) Lietti, L.; Nova, I.; Forzatti, P. Selective catalytic reduction (SCR) of NO by NH<sub>3</sub> over TiO<sub>2</sub>-supported V<sub>2</sub>O<sub>5</sub>-WO<sub>3</sub> and V<sub>2</sub>O<sub>5</sub>-MoO<sub>3</sub> catalysts. *Top. Catal.* **2000**, *11–12*, 111–122.
- (7) Zhu, H.; Dong, C.; Wang, X.; Zhu, Y.; Shen, C.; Zhang, X.; Qin, W.; Hu, X.; Zhang, J.; Wang, X.; Zhao, Y.; Xue, J. PREPARATION AND PROPERTIES OF V-Mo/TiO<sub>2</sub> CORDIERITE SUPPORTED DENITRATION CATALYST. *Environ. Eng.* **2020**, *38*, 168–174. (in Chinese)
- (8) Casagrande, L.; Lietti, L.; Nova, I.; Forzatti, P.; Baiker, A. SCR of NO by NH<sub>3</sub> over TiO<sub>2</sub>-supported V<sub>2</sub>O<sub>5</sub>-MoO<sub>3</sub> catalysts: reactivity and redox behavior. *Appl. Catal., B* **1999**, *22*, 63–77.
- (9) Saracco, G.; Specchia, V. Simultaneous removal of nitrogen oxides and fly-ash from coal-based power-plant flue gases. *Appl. Therm. Eng.* **1998**, *18*, 1025–1035.
- (10) Kamble, P.; Unnikrishnan, S.; Khot, S.; Ananthanarayanan, A.; Banerjee, D.; Gopalakrishnan, S.; Shah, J.; Agarwal, K. Development of De-NO<sub>x</sub> selective catalytic reduction catalyst using V<sub>2</sub>O<sub>5</sub>-TiO<sub>2</sub> supported on a ceramic filter candle. *Int. J. Environ. Stud.* **2019**, *76*, 306–317.
- (11) Choi, J.-H.; Kim, J.-H.; Bak, Y.-C.; Amal, R.; Scott, J. Pt-V<sub>2</sub>O<sub>5</sub>-WO<sub>3</sub>/TiO<sub>2</sub> catalysts supported on SiC filter for NO reduction at low temperature. *Korean J. Chem. Eng.* **2005**, *22*, 844–851.
- (12) Hackel, M.; Schaub, G.; Nacken, M.; Heidenreich, S. Kinetics of reduction and oxidation reactions for application in catalytic gas-particle-filters. *Powder Technol.* **2008**, *180*, 239–244.
- (13) Heidenreich, S.; Nacken, M.; Hackel, M.; Schaub, G. Catalytic filter elements for combined particle separation and nitrogen oxides removal from gas streams. *Powder Technol.* **2008**, *180*, 86–90.
- (14) Nacken, M.; Heidenreich, S.; Hackel, M.; Schaub, G. Catalytic activation of ceramic filter elements for combined particle separation,

NO<sub>x</sub> removal and VOC total oxidation. *Appl. Catal., B* **2007**, *70*, 370–376.

(15) Zürcher, S.; Hackel, M.; Schaub, G. Kinetics of selective catalytic NO<sub>x</sub> reduction in a novel gas-particle filter reactor (catalytic filter element and sponge insert). *Ind. Eng. Chem. Res.* **2008**, *47*, 1435–1442.

(16) Wang, R.; Zhao, L.; Hu, X.; Liu, Z.; Zhang, H.; Jin, J. Study on V<sub>2</sub>O<sub>5</sub>-WO<sub>3</sub>-TiO<sub>2</sub> catalytic filter for de-NO and particle separation. *Mater. Res. Express* **2019**, *6*, 115512.

(17) Kim, Y. A.; Choi, J. H.; Scott, J.; Chiang, K.; Amal, R. Preparation of high porous Pt-V<sub>2</sub>O<sub>5</sub>-WO<sub>3</sub>/TiO<sub>2</sub>/SiC filter for simultaneous removal of NO and particulates. *Powder Technol.* **2008**, *180*, 79–85.

(18) Fino, D.; Russo, N.; Saracco, G.; Specchia, V. A multifunctional filter for the simultaneous removal of fly-ash and NO<sub>x</sub> from incinerator flue gases. *Chem. Eng. Sci.* **2004**, *59*, 5329–5336.

(19) Peng, Y.; Si, W.; Li, X.; Luo, J.; Li, J.; Crittenden, J.; Hao, J. Comparison of MoO<sub>3</sub> and WO<sub>3</sub> on arsenic poisoning V<sub>2</sub>O<sub>5</sub>/TiO<sub>2</sub> catalyst: DRIFTS and DFT study. *Appl. Catal., B* **2016**, *181*, 692–698.

(20) Kobayashi, M.; Kuma, R.; Morita, A. Low temperature selective catalytic reduction of NO by NH<sub>3</sub> over V<sub>2</sub>O<sub>5</sub> supported on TiO<sub>2</sub>-SiO<sub>2</sub>-MoO<sub>3</sub>. *Catal. Lett.* **2006**, *112*, 37–44.

(21) Qiu, Y.; Liu, B.; Du, J.; Tang, Q.; Liu, Z.; Liu, R.; Tao, C. The monolithic cordierite supported V<sub>2</sub>O<sub>5</sub>-MoO<sub>3</sub>/TiO<sub>2</sub> catalyst for NH<sub>3</sub>-SCR. *Chem. Eng. J.* **2016**, *294*, 264–272.

## Recommended by ACS

### Follow-up Research on Simultaneous Removal of NO and SO<sub>2</sub> by Wet Scrubbing NaClO Solution Combined In Situ with Ozone Oxidation: Performance and Mechanism

Junqi Cheng, Xinxiang Pan, *et al.*

OCTOBER 23, 2022

INDUSTRIAL & ENGINEERING CHEMISTRY RESEARCH

READ 

### Insights into Coproduction of Silica Gel via Desulfurization of Steel Slag and Silica Gel Adsorption Performance

Zhuohui Ma, Fangqin Cheng, *et al.*

JUNE 09, 2022

ACS OMEGA

READ 

### Causes and Control Technology of Slurry Overflow in an Ammonia Desulfurization Tower

Xiaodong Chen, Xufei Chen, *et al.*

SEPTEMBER 22, 2021

ACS OMEGA

READ 

### Enrichment Mechanism of Lithium in Late Permian Coals in the Bijie Area, Guizhou, China

Qingwei Wang, Fengying Zhou, *et al.*

MAY 02, 2022

ACS OMEGA

READ 

Get More Suggestions >